

Finite Volume Formulation of the MIB Method for Elliptic Interface Problems

Yin Cao¹, Bao Wang¹, Kelin Xia¹, and Guowei Wei^{1,2} *

¹*Department of Mathematics, Michigan State University, East Lansing, MI 48824, USA*

²*Department of Electrical and Computer Engineering,
Michigan State University, East Lansing, MI 48824, USA*

October 9, 2018

Abstract

The matched interface and boundary (MIB) method has a proven ability for delivering the second order accuracy in handling elliptic interface problems with arbitrarily complex interface geometries. However, its collocation formulation requires relatively high solution regularity. Finite volume method (FVM) has its merit in dealing with conservation law problems and its integral formulation works well with relatively low solution regularity. We propose an MIB-FVM to take the advantages of both MIB and FVM for solving elliptic interface problems. We construct the proposed method on Cartesian meshes with vertex-centered control volumes. A large number of numerical experiments are designed to validate the present method in both two dimensional (2D) and three dimensional (3D) domains. It is found that the proposed MIB-FVM achieves the second order convergence for elliptic interface problems with complex interface geometries in both L_∞ and L_2 norms.

Keywords: Elliptic interface problem; Complex interface geometry; Finite volume method; Matched interface and boundary.

*Corresponding author. Tel: (517)353 4689, Fax: (517)432 1562, Email: wei@math.msu.edu

1 Introduction

Elliptic partial differential equations (PDEs) with discontinuous coefficients and singular source terms, commonly referred to as elliptic interface problems, occur in many applications, including fluid dynamics [11, 25, 32, 31], material science [22], electromagnetics [19, 21, 28, 66], biological systems, [16, 37, 60, 67, 7] and heat or mass transfer [15]. Since the pioneer work of Peskin in 1977 [45], lots of attention has been paid to this field in the past few decades [2, 5, 10, 13, 24, 23, 26, 27, 29, 32, 36, 39, 46, 47, 49, 50, 42, 55, 6].

An elliptic interface problem is formulated as elliptic PDEs defined on piecewise-smooth subdomains, which are coupled together via interface conditions, such as given jumps in solution and flux across the domain interface. Without the interface, a large variety of convergent numerical schemes are available for solving the elliptic PDEs, such as, finite difference method (FDM), finite element method (FEM), finite volume method (FVM), wavelet, radial basis functions, meshless and spectral methods. However, for elliptic interface problems, the direct application of the aforementioned schemes cannot yield a convergent solution.

Peskin proposed the immersed boundary method (IBM) [17, 30, 45] in order to simulate flow pattern of blood in the heart, in which he approximated the singular sources on the interface. Since his work, many numerical methods have been proposed and studied. In 1984, Mayo introduced a second order integral equation approach for Poisson's equation and biharmonic equation on irregular domains [40, 41], in which the solution is extended to a rectangular region by using Fredholm integral equations. A fast Poisson solver is utilized to solve the resulting Fredholm integral equations on a rectangular region. Continuous derivatives have been assumed to evaluate the discrete Laplacian. This method can deal with jump conditions of $[u] \neq 0$ and $[u_n] = 0$ when the Green's function is available. In 1994, a level set method in combination with the immersed boundary method [48] is proposed by Osher and his coworkers in order to compute solutions to incompressible two-phase flow. This level set method is easy to implement, although it is of low convergent rate. In the same year, immersed interface method (IIM) was proposed by Levique and Li [33, 34, 1], in which the interface conditions are incorporated into the finite difference scheme near the interface to achieve second order accuracy based on a Taylor expansion in a local coordinate system. It is a second order interface scheme that does not smear the interface jumps and is used to solve elliptic and parabolic interface problems alike. The resulting linear system is sparse, but not symmetric or positive definite. Also, second order derivatives of the interface jumps are needed. The IIM is widely used in practice and its extensions can be seen in Refs. [34, 1]. For instance, in 2001, Li and Ito [34] constructed an IIM scheme with resulting linear matrix being diagonally dominate and its symmetric part being negative definite.

In addition to the IIM, a large class of finite difference based numerical methods have also been proposed for solving elliptic interface problem. The crucial idea of these methods is to incorporate jump conditions into the difference stencils near the interface to maintain high order local truncation error using Taylor expansion. Numerical schemes based on finite element or finite volume are also developed [44, 35, 20]. Finite element schemes are usually constructed by modifying the finite element basis near the interface. A few methods on unfitted mesh have been introduced based on the discontinuous Galerkin method using interior penalty technique to handle jump and flux conditions [3, 18]. The weak Galerkin finite element method has also been developed for elliptic interface problem [43]. Other interesting methods developed in recent decades include the ghost fluid method (GFM) by Fedkiw, Osher and coworkers [12, 38]. The second order convergence of finite difference formalism of interface methods is proved in 2006 by Beale and Layton for smooth interface [4], whereas convergence analysis of most elliptic interface schemes is yet to be done.

In the past decade, we have dedicated ourselves to designing accurate and robust numerical schemes for solving elliptic interface problems. In 2006, the matched interface and boundary (MIB) method [63, 61, 70, 69] was proposed, motivated by many practical needs, such as optical molecular imaging [8], nano-electronic devices, [8], vibration analysis of plates [62], wave propagation [65, 64], geodynamics [68] and electrostatic potential in proteins [67, 60, 16, 7]. One important feature of the MIB method is its extension of computational domains by using the so called fictitious values, an strategy developed in our earlier methods for handling boundaries [53, 54] and interfaces [66]. As such, standard central

finite difference schemes can be employed to discretize differential operators as if there were no interface. Another unique feature of the MIB method is to repeatedly enforce only the lowest order jump conditions to achieve higher order convergence, which is of critical importance for the robustness of the method to deal with arbitrarily complex interface geometries. Higher-order jump conditions must involve higher order derivatives and/or cross derivatives. Therefore, to approximate higher order derivatives and/or cross derivatives, one must utilize larger stencils, which is unstable for constructing high-order interface schemes and cumbersome for complex interface geometries. The other distinct feature of the MIB method is its dimensional splitting. To enforce a 2D or 3D interface jump condition, we divide the problem into multi 1D ones and resolve a 1D problem at a time, if possible. This approach enables us to come up with a systematic procedure to resolve high dimensional interface problems. Finally, based on high order Lagrange polynomials, the MIB method is of arbitrarily high order in principle. For example, MIB schemes up to 16th order accurate have been constructed for simple interface geometries 1D and 2D domains [66, 70], and sixth-order accurate MIB schemes have been developed for complex interfaces in 2D [70] and 3D domains [61, 70]. Recently we have constructed an adaptively deformed mesh based MIB [57] and a Galerkin formulation of MIB [59, 56] to improve MIB's capability of solving realistic problems. A comparison of the GFM, IIM and MIB methods can be found in in Refs. [70, 69].

The MIB method has been used in our earlier works for solving many scientific and engineering problems, such as Poisson-Boltzmann equation (PBE) [67, 60, 16, 7] for describing the electrostatic potential in proteins. To our best knowledge, the MIB method is the only method that has demonstrated the second order accuracy for solving Poisson or PB equation with realistic protein surfaces with geometric singularities [60, 16, 7] and for solving Poisson equation with multiple material interfaces [58]. It can also be used to solve the Helmholtz equation for wave scattering and propagation in inhomogeneous media. A fourth order MIB scheme for the Helmholtz equation with arbitrarily curved interfaces has been proposed by Zhao [65, 64]. Another example is the geodynamics where the Navier-Stokes equations with discontinuous viscosity and density is to be solved. Zhou *et al* have developed a second order accurate MIB method to solve this problem on non-staggered Cartesian grids [68]. Furthermore, the elastic interface problem in both 2D and 3D domains with arbitrarily complex interface geometry was also addressed by the MIB method [51, 52]. In the past few years, the MIB method has also been applied to the optical molecular imaging [9], nano-electronic devices, [8] and vibration analysis of plates [62].

Due to the importance and complexity of interface problems, it is still urgent to develop methods that are more accurate, robust and require less computational cost. Finite volume method (FVM) is known for its ability to better conserve mass and flux in conservation law problems. This property is fundamental for the simulation of many physical models, e.g., oil recovery simulation and computational fluid dynamics in general. Additionally, compared with finite difference method which takes a collocation formulation, FVM is able to deal with solutions with relatively lower regularity. In the present work, we propose the finite volume formulation of the MIB method (MIB-FVM). The motivation for the proposed MIB-FVM is to inherit the merits of both methods, namely, the capability of the MIB method in handling complex interface geometries and the advantage of FVM for conservation laws and low solution regularity.

The rest of this paper is organized as the follows. In Section 2, the general theory of the MIB based finite volume formulation is briefly discussed. The theoretical formulation and the computational algorithms are given as well. In Section 3, we present the strategy for treating complex interface geometries. In Section 4, the proposed MIB-FVM is validated by benchmark tests, such as 6-petal flower and jigsaw puzzle-like shape in two dimensional (2D) space, and sphere, ellipsoid, cylinder, flower-based cylinder and torus in three dimensional (3D) space. Solutions of less regularity (H^2 continuous) are also tested for the spherical and ellipsoidal interface in 3D. This paper ends with a conclusion.

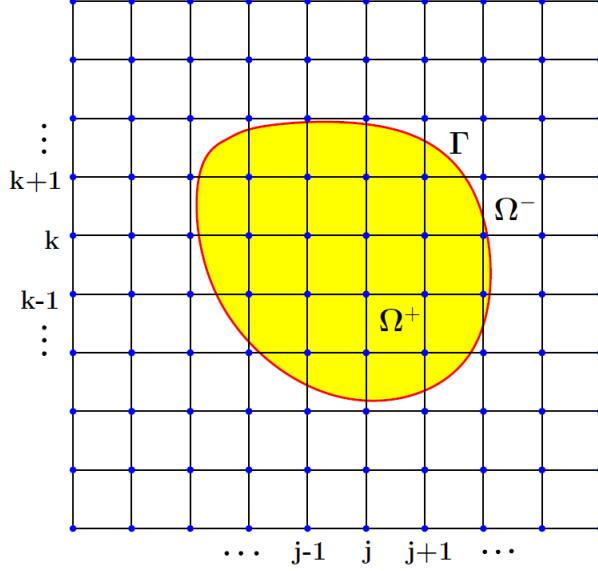


Figure 1: Illustration of a 3D interface problem at a cross section. The whole domain Ω is divided by interface Γ into two subdomains, Ω^+ and Ω^- . The mesh is represented by solid lines. The grid points are represented by blue dots.

2 Matched interface and boundary - finite volume method (MIB-FVM)

Let us consider an open bounded domain $\Omega \subset \mathbb{R}^3$ with a given interface Γ , which separates the domain into two subdomains, Ω^+ and Ω^- as illustrated in Figure 1.

The boundary $\partial\Omega$ and interfaces Γ may be non-smooth. The interface can be characterized by a piecewise smooth level-set function $\varphi \in \Omega$, such that $\Gamma = \{\mathbf{x} | \varphi(\mathbf{x}) = 0, \forall \mathbf{x} \in \Omega\}$. As such, two subdomains can be given by $\Omega^+ = \{\mathbf{x} | \varphi(\mathbf{x}) < 0, \forall \mathbf{x} \in \Omega\}$ and $\Omega^- = \{\mathbf{x} | \varphi(\mathbf{x}) > 0, \forall \mathbf{x} \in \Omega\}$. The elliptic interface problem can be formulated as

$$-\nabla \cdot \beta(\mathbf{x}) \nabla u(\mathbf{x}) = g(\mathbf{x}), \quad \forall \mathbf{x} \in \Omega \quad (1)$$

$$u = g_b, \quad \forall \mathbf{x} \text{ on } \partial\Omega, \quad (2)$$

where $g(\mathbf{x})$ is a piecewise continuous function, g_b is the boundary value, and $\beta(\mathbf{x})$ is a variable coefficient that is discontinuous across the interface Γ . As a result, two jump conditions are required to make the problem well posed

$$[u] = u^+ - u^- = \Phi, \quad \forall \mathbf{x} \text{ on } \Gamma \quad (3)$$

and

$$[\beta u_n] = \beta^+ u_n^+ - \beta^- u_n^- = \Psi, \quad \forall \mathbf{x} \text{ on } \Gamma, \quad (4)$$

where u^+, u_n^+ and β^+ denote their limiting value from the Ω^+ side of the interface Γ , and u^-, u_n^- and β^- denote their limiting value from the Ω^- side of the interface Γ . The derivatives u_n^+ and u_n^- are evaluated along the outer normal direction on the interface. Here $\Phi(\mathbf{x})$ and $\Psi(\mathbf{x})$ is at least C^1 continuous. Equations (1)-(4) define the elliptic interface problem to be solved in the present work.

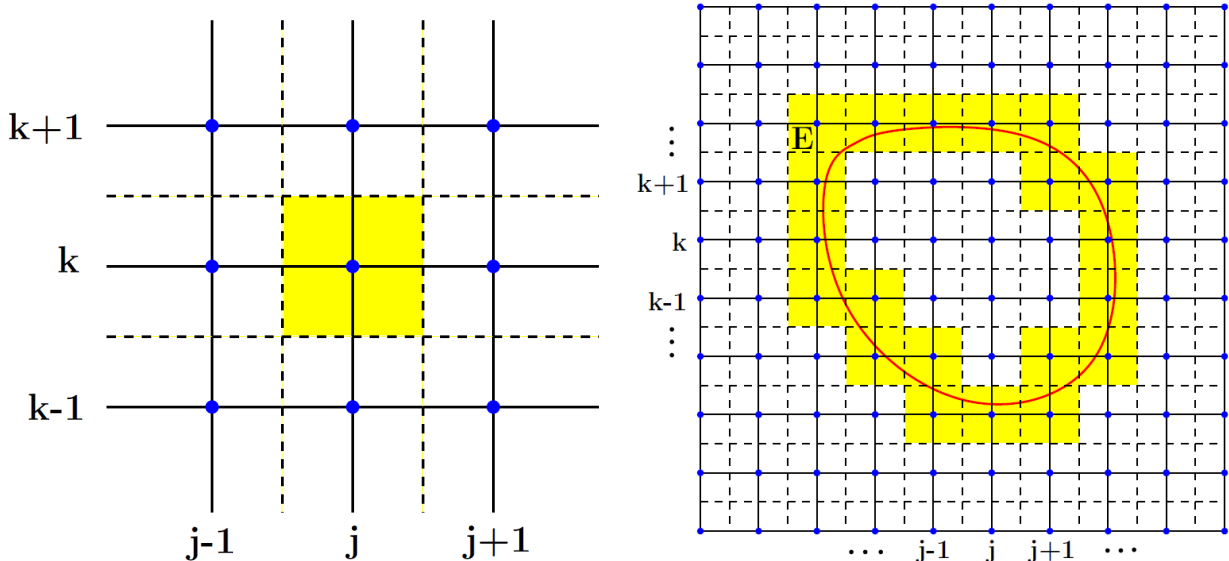


Figure 2: Left chart: Illustration of the 3D control volume at a cross section that is perpendicular to the x -axis and intersect with the x -axis at the i th grid point. The yellow region denotes the control volume associated with the grid point (i, j, k) . The grid points are denoted by blue dots. The mesh is represented by solid lines and the dual mesh is represented by the dashed lines. Right chart: Illustration of the 3D irregular domain E at a cross section. The irregular domain is denoted by the yellow region. The grid points are denoted by blue dots. The mesh is represented by solid lines and the dual mesh is represented by dashed lines.

2.1 Introduction to the MIB finite volume method

To avoid the time-consuming mesh generation procedure, like the original MIB method, we employ the Cartesian mesh. We also employ the vertex-centered finite volume method, which means that we associate control volumes and unknowns to vertices. The control volumes are cubes whose centers are located at the grid points and whose sides intercept at the midpoints between grid points, which is illustrated by the left chart of Figure 2.

Like the original MIB method, the grid points and control volumes are classified into regular and irregular types. A grid point is said to be irregular if the standard central finite difference (CFD) scheme at the grid point near the interface requires grid point(s) from the other side of the interface. In Figure 1, the interface Γ and the different domains Ω , Ω^+ and Ω^- are depicted. As is shown in the figure, the complex interface inevitably cut through certain control volumes. A control volume is defined to be irregular if it is cut through by the interface, or stated differently, the vertices of the control volume locate on both side of the interface. The irregular domain E is defined to be the union of all irregular control volumes, as is shown in the right chart of Figure 2.

In the present MIB-FVM, we further define each control volume to be a positive or negative control volume according to where its center is, i.e., a control volume is said a positive one if its center grid point locates in the positive region Ω^+ ; similarly, a control volume is said a negative one if its center grid point locates in the negative region Ω^- . We also define Ω_o^+ and Ω_o^- to be the union of all positive and negative control volumes, respectively, as is shown in Figure 3. Domain Ω_o^+ and Ω_o^- can be viewed as the generalized Ω^+ and Ω^- . First, domains Ω_o^+ and Ω_o^- are disjoint by such definition; secondly, it can be easily seen that there is no inclusion relation between the origin subdomains Ω^+ or Ω^- and the generalized subdomains Ω_o^+ or Ω_o^- .

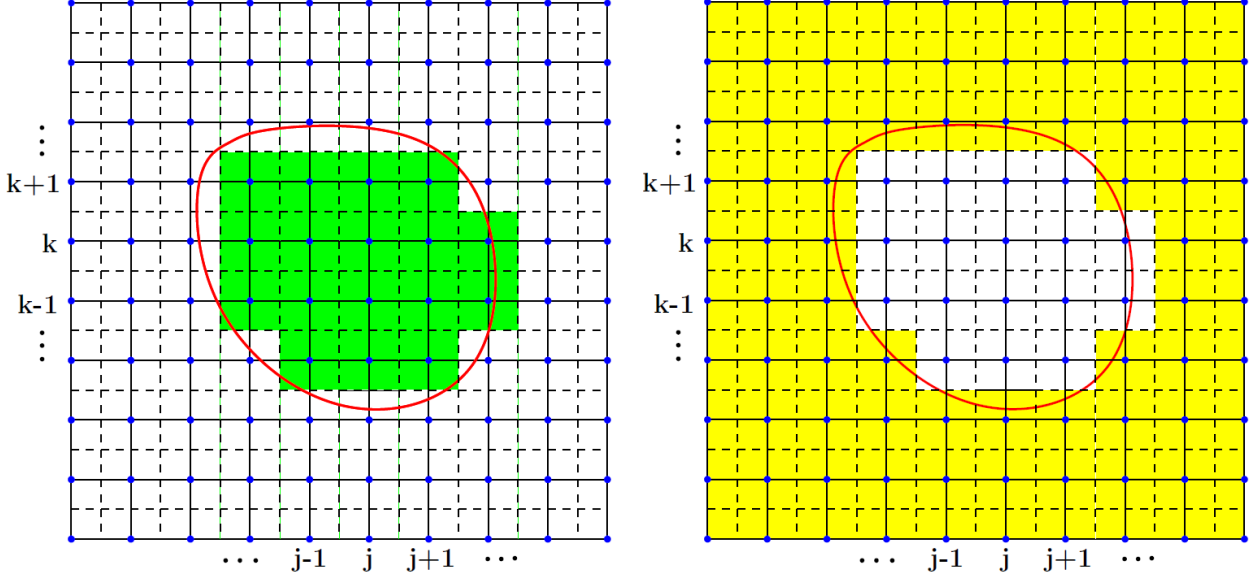


Figure 3: Illustration of the domain re-division at a cross section. Left chart: domain Ω_o^+ (in green), which is the union of all the positive control volumes; Right chart: domain Ω_o^- (in yellow), which is the union of all the negative control volumes.

To properly define the elliptic interface problem, we also need to generalize the discontinuous coefficient $\beta(\mathbf{x})$ and the source term $g(\mathbf{x})$ over the generalized domains. To this end, we define

$$\beta_o^+(\mathbf{x}) = \begin{cases} \beta^+(\mathbf{x}), & \forall \mathbf{x} \in \Omega_o^+ \cap \Omega^+ \\ \beta_{ex}^+(\mathbf{x}), & \forall \mathbf{x} \in \Omega_o^+ \cap \Omega^{+c} \end{cases} \quad (5)$$

and

$$\beta_o^-(\mathbf{x}) = \begin{cases} \beta^-(\mathbf{x}), & \forall \mathbf{x} \in \Omega_o^- \cap \Omega^- \\ \beta_{ex}^-(\mathbf{x}), & \forall \mathbf{x} \in \Omega_o^- \cap \Omega^{-c}, \end{cases} \quad (6)$$

where $\beta_{ex}^+(\mathbf{x})$ and $\beta_{ex}^-(\mathbf{x})$ are the smooth extensions of the coefficients $\beta^+(\mathbf{x})$ and $\beta^-(\mathbf{x})$ over domains Ω_o^+ and Ω_o^- , respectively. The superscript c means complement.

Similarly, we define

$$g_o^+(\mathbf{x}) = \begin{cases} g^+(\mathbf{x}), & \forall \mathbf{x} \in \Omega_o^+ \cap \Omega^+ \\ g_{ex}^+(\mathbf{x}), & \forall \mathbf{x} \in \Omega_o^+ \cap \Omega^{+c} \end{cases} \quad (7)$$

and

$$g_o^-(\mathbf{x}) = \begin{cases} g^-(\mathbf{x}), & \forall \mathbf{x} \in \Omega_o^- \cap \Omega^- \\ g_{ex}^-(\mathbf{x}), & \forall \mathbf{x} \in \Omega_o^- \cap \Omega^{-c}, \end{cases} \quad (8)$$

where g_{ex}^+ and g_{ex}^- are the smooth extension of the functions $g^+(\mathbf{x})$ and $g^-(\mathbf{x})$ over domains Ω_o^+ and Ω_o^- , respectively. The superscript c denotes complement.

By doing the generalization above, we can define the original interface problems on irregular control volumes. As the solution and its gradient can be discontinuous across the interface, to solve the interface

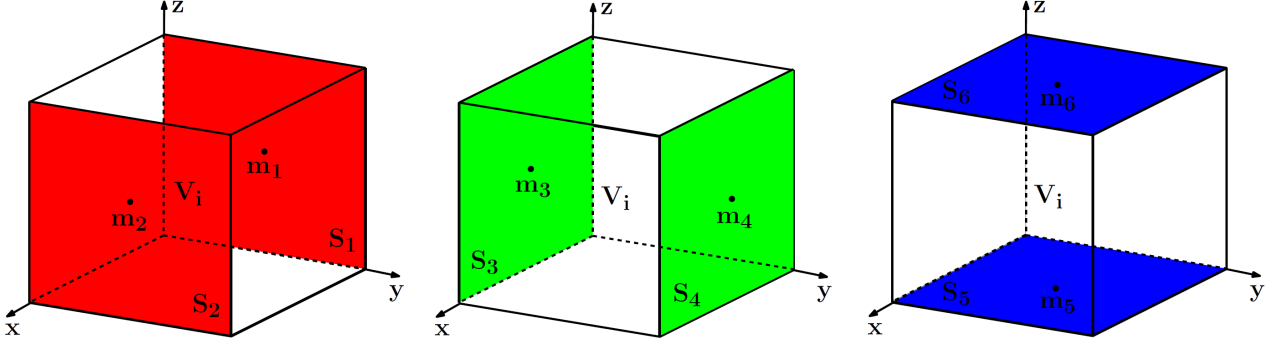


Figure 4: Illustration of the faces of control volume V_i . Left chart: S_1 and S_2 are two faces along the x -direction; middle chart: S_3 and S_4 are two faces along the y -direction; right chart: S_5 and S_6 are two faces along the z -direction. m_i is the center of S_i , where $i = 1, 2, \dots, 6$.

problem, one needs to rigorously enforce the interface jump conditions. These conditions, interpreted by a set of equations, are utilized to determine fictitious values on generalized domains numerically. The detailed procedure of computing fictitious values is described in Section 3. To achieve high order finite difference type of MIB schemes, the set of interface conditions are iteratively implemented to determine as many fictitious values as needed. This approach can also be used to create a high-order MIB-FVM.

2.2 MIB finite volume formulation

The MIB-FVM is based on the **integral form** rather than the **differential form** of Eq. (1). The integral form of the equation can be obtained by taking integral on both sides of the equation over any control volume V_i and using the divergence theorem on the left hand side

$$\int_{\partial V_i} \beta(\mathbf{x}) \nabla u(\mathbf{x}) \cdot \mathbf{n} dS = \int_{V_i} g(\mathbf{x}) d\mathbf{x}, \quad (9)$$

where ∂V_i denotes the surface of the control volume V_i , and \mathbf{n} denotes the unit outer normal vector of ∂V_i .

The above equation can be written as

$$\int_{\partial V_i} (\beta u_x, \beta u_y, \beta u_z) \cdot (n_1, n_2, n_3) dS = \int_{V_i} g(\mathbf{x}) d\mathbf{x}, \quad (10)$$

where (n_1, n_2, n_3) is the coordinate of the unit outer normal \mathbf{n} .

As is illustrated in Figure 4, since the control volume V_i is a cube, ∂V_i consists of 6 faces, denoted by ∂S_i where $i = 1, 2, \dots, 6$. For instance, ∂S_1 denotes the left face, whose unit outer normal is $(-1, 0, 0)$; ∂S_2 denotes the right face, whose unit outer normal is $(1, 0, 0)$, and so on.

As a result, Eq. (10) can be further written as

$$-\int_{\partial S_1} \beta u_x dS + \int_{\partial S_2} \beta u_x dS - \int_{\partial S_3} \beta u_y dS + \int_{\partial S_4} \beta u_y dS - \int_{\partial S_5} \beta u_z dS + \int_{\partial S_6} \beta u_z dS = \int_{V_i} g(\mathbf{x}) d\mathbf{x}. \quad (11)$$

The above surface and volume integrals are further approximated by Gauss quadrature rules. In practice, we use the second order midpoint rule, thus the surface integrals on the left hand side are approximated by the function values at the face center, times the face area; the volume integral on the

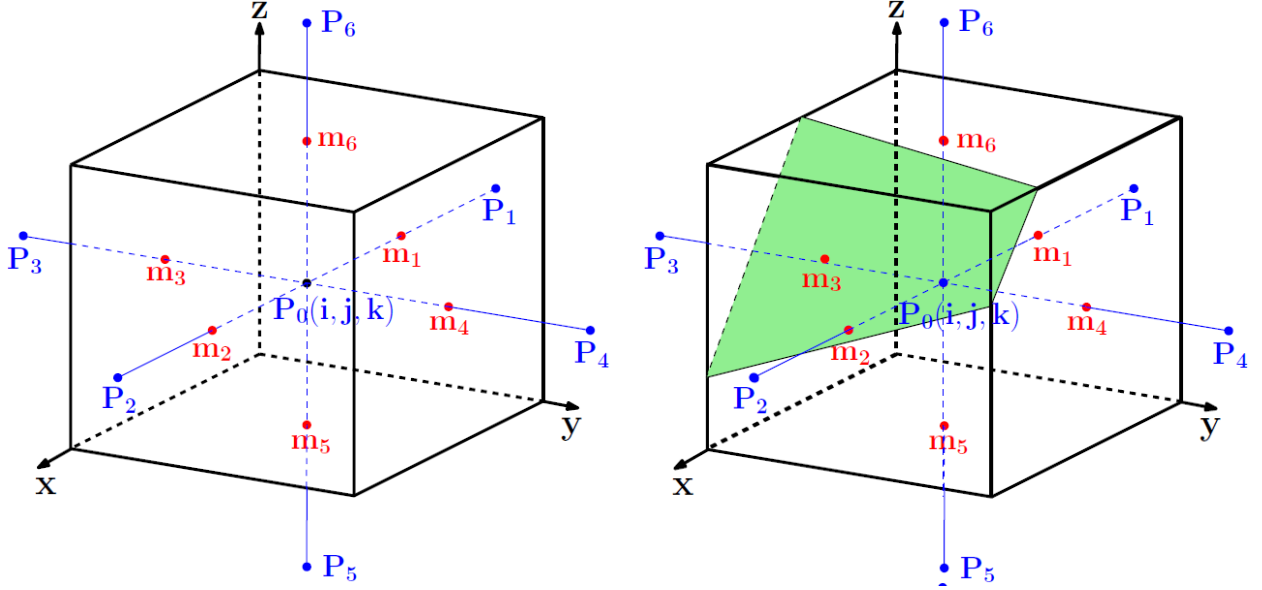


Figure 5: Exemplary configurations for a regular control volume on the left and an irregular one on the right. Here $P_i, i = 0, 1, 2, \dots, 6$ in blue color denote the grid points, with P_0 being the center of the control volume. Here $m_i, i = 1, 2, \dots, 6$ in red color denote the centers of the corresponding faces. For the right chart, the green area represents the 2D interface in 3D that divides the control volume into two parts.

right hand side is approximated by the function value at the center, times the volume of the control volume. Based on Figure 5 and the midpoint rule, Eq. (11) can be further written as

$$-(\beta u_x)_{m_1} dydz + (\beta u_x)_{m_2} dydz - (\beta u_y)_{m_3} dx dz + (\beta u_y)_{m_4} dx dz - (\beta u_z)_{m_5} dx dy + (\beta u_z)_{m_6} dx dy = g_i dx dy dz, \quad (12)$$

where $(\beta u_t)_{m_i}, t = x, y, z; i = 1, 2, \dots, 6$ denote the function value of (βu_t) at the i th midpoint m_i ; g_i denote the function value of $g(\mathbf{x})$ at the center of the i th control volume V_i ; and dx, dy and dz denote the size of partition in x, y and z direction, respectively.

For a regular control volume illustrated by the left chart of Figure 5, the above partial derivatives at the midpoints can be evaluated by a 3-point interpolation scheme, namely

$$\begin{aligned} (\beta u_x)_{m_1} &\approx (\beta)_{m_1} \cdot (w_1^1, w_1^2, w_1^3) \cdot (u_{i-1,j,k}, u_{i,j,k}, u_{i+1,j,k})^T \\ (\beta u_x)_{m_2} &\approx (\beta)_{m_2} \cdot (w_2^1, w_2^2, w_2^3) \cdot (u_{i-1,j,k}, u_{i,j,k}, u_{i+1,j,k})^T \\ (\beta u_y)_{m_3} &\approx (\beta)_{m_3} \cdot (w_3^1, w_3^2, w_3^3) \cdot (u_{i,j-1,k}, u_{i,j,k}, u_{i,j+1,k})^T \\ (\beta u_y)_{m_4} &\approx (\beta)_{m_4} \cdot (w_4^1, w_4^2, w_4^3) \cdot (u_{i,j-1,k}, u_{i,j,k}, u_{i,j+1,k})^T \\ (\beta u_z)_{m_5} &\approx (\beta)_{m_5} \cdot (w_5^1, w_5^2, w_5^3) \cdot (u_{i,j,k-1}, u_{i,j,k}, u_{i,j,k+1})^T \\ (\beta u_z)_{m_6} &\approx (\beta)_{m_6} \cdot (w_6^1, w_6^2, w_6^3) \cdot (u_{i,j,k-1}, u_{i,j,k}, u_{i,j,k+1})^T \end{aligned} \quad (13)$$

where $w_i^j, i = 1, 2, \dots, 6; j = 1, 2, 3$ are the interpolation weights, and $u_{i,j,k}$ denotes the function value at grid point (i, j, k) .

For an irregular control volume illustrated by the right chart of Figure 5, to maintain the same

convergence rate and accuracy, the above interpolations must be modified as

$$\begin{aligned}
(\beta u_x)_{m_1} &\approx (\beta_o)_{m_1} \cdot (w_1^1, w_1^2, w_1^3) \cdot (\tilde{u}_{i-1,j,k}, u_{i,j,k}, \tilde{u}_{i+1,j,k})^T \\
(\beta u_x)_{m_2} &\approx (\beta_o)_{m_2} \cdot (w_2^1, w_2^2, w_2^3) \cdot (\tilde{u}_{i-1,j,k}, u_{i,j,k}, \tilde{u}_{i+1,j,k})^T \\
(\beta u_y)_{m_3} &\approx (\beta_o)_{m_3} \cdot (w_3^1, w_3^2, w_3^3) \cdot (\tilde{u}_{i,j-1,k}, u_{i,j,k}, \tilde{u}_{i,j+1,k})^T \\
(\beta u_y)_{m_4} &\approx (\beta_o)_{m_4} \cdot (w_4^1, w_4^2, w_4^3) \cdot (\tilde{u}_{i,j-1,k}, u_{i,j,k}, \tilde{u}_{i,j+1,k})^T \\
(\beta u_z)_{m_5} &\approx (\beta_o)_{m_5} \cdot (w_5^1, w_5^2, w_5^3) \cdot (\tilde{u}_{i,j,k-1}, u_{i,j,k}, \tilde{u}_{i,j,k+1})^T \\
(\beta u_z)_{m_6} &\approx (\beta_o)_{m_6} \cdot (w_6^1, w_6^2, w_6^3) \cdot (\tilde{u}_{i,j,k-1}, u_{i,j,k}, \tilde{u}_{i,j,k+1})^T
\end{aligned} \tag{14}$$

where β_o denotes the generalization of β defined in Eqs. (5) and (6), and \tilde{u} is defined as

$$\tilde{u}_{x,y,z} = \begin{cases} u_{x,y,z} & \text{if } (x, y, z) \text{ is on the same side of the interface with } (i, j, k) \\ f_{x,y,z} & \text{if } (x, y, z) \text{ is on different side of the interface with } (i, j, k). \end{cases}$$

Here $f_{x,y,z}$ represents the fictitious value at grid point (x, y, z) , which is computed by MIB method. The detailed procedure of determining these fictitious values are described in the next section.

3 Algorithms for determining fictitious values

3.1 Simplification of interface jump conditions

To solve the above linear equation system, we need to determine the involved fictitious values first. This issue is discussed in the present section. We first describe the interface jump conditions, which are needed at each intersecting point of control volume edges and the interface.

As the interface normal direction varies along the interface, which is very troublesome from the computational point of view. We introduce a local coordinate system at each intersection point of the Cartesian mesh and the interface to treat different interface geometries systematically. At a specific intersection point, the local coordinate system is denoted by (ξ, η, ζ) , where ξ denotes the normal direction and η is on the $x-y$ plane. The relation of the local coordinates and the Cartesian coordinates is described in the following

$$\begin{pmatrix} \xi \\ \eta \\ \zeta \end{pmatrix} = \mathbf{P} \cdot \begin{pmatrix} x \\ y \\ z \end{pmatrix} \tag{15}$$

where \mathbf{P} is the transformation matrix

$$\mathbf{P} = \begin{pmatrix} \sin \phi \cos \theta & \sin \phi \sin \theta & \cos \phi \\ -\sin \theta & \cos \theta & 0 \\ -\cos \phi \cos \theta & -\cos \phi \sin \theta & \sin \phi \end{pmatrix}, \tag{16}$$

where θ and ϕ are the azimuth and zenith angles with respect to the normal direction \mathbf{n} , respectively.

Without generating higher order jump conditions, usually we differentiate Eq. (3) in two tangential directions in order to obtain two additional jump conditions $[u_\eta] = u_\eta^+ - u_\eta^-$, and $[u_\zeta] = u_\zeta^+ - u_\zeta^-$. Thus, in the new coordinate system, the jump conditions in two tangential directions can be discretized as

$$[u_\eta] = (-\sin \theta u_x^+ + \cos \theta u_y^+) - (-\sin \theta u_x^- + \cos \theta u_y^-) \tag{17}$$

$$[u_\zeta] = (-\cos \phi \cos \theta u_x^+ - \cos \phi \sin \theta u_y^+ + \sin \phi u_z^+) - (-\cos \phi \cos \theta u_x^- - \cos \phi \sin \theta u_y^- + \sin \phi u_z^-). \tag{18}$$

Similarly, in the new coordinate system, the jump condition Eq. (4) can be discretized as

$$[\beta u_\xi] = \beta^+ (\sin \phi \cos \theta u_x^+ + \sin \phi \sin \theta u_y^+ + \cos \phi u_z^+) - \beta^- (\sin \phi \cos \theta u_x^- + \sin \phi \sin \theta u_y^- + \cos \phi u_z^-). \tag{19}$$

These jump conditions, together with the original jump condition Eq. (3), constitutes a set of lowest order jump conditions that is enforced in the MIB method.

In principle, by differentiating these lowest order jump conditions, we can generate even more jump conditions. However by doing this, we could create some higher-order derivatives and cross derivatives, whose evaluation often involves larger stencils, which is unstable for constructing high-order numerical schemes and unfeasible for truly complex interface geometries. Therefore, the spirit of the original MIB method is to use only the lowest order interface jump conditions. This spirit is preserved in the proposed MIB-FVM. We only use jump conditions in Eqs. (3), (17), (18) and (19).

Thus, at each intersection of the interface and the mesh line, there are four jump conditions described by Eqs. (3), (17), (18) and (19), which involve the function values and only the first order derivatives. This property is very important for making the numerical scheme more stable and efficient in handling complex interface geometries. Besides, employing only the lowest derivatives will generate a more-banded matrix with a smaller conditional number. The enforcement of these jump conditions determines fictitious values to be used in the discretization of differential operators in a given PDE.

The discretization of the differential operator involves six partial derivatives, namely $\frac{\partial u^\pm}{\partial x_j}$, where $x_j = x, y, z$. In dealing with complex interface geometries, some of these partial derivatives could be very difficult or even impossible to be approximated with some given order of accuracy. Since in constructing a second order numerical scheme, there is a pair of fictitious values along each mesh line and they are solved simultaneously, with the aforementioned four jump conditions, it is affordable for us to eliminate two of them. This redundancy gives two more degrees of freedom for us to design efficient and robust second order schemes in handling complex interface geometries. The designed numerical scheme systematically eliminates the two partial derivatives that are most difficult to discretize at each intersection of the interface and the mesh line by using two redundant jump conditions. In summary, at each intersection of the interface and the mesh line, there are four remaining partial derivatives that are need to be discretized.

The elimination process must comply with the following rules:

- All fictitious values on all irregular points are determined. At the intersection of the interface and each mesh line, two fictitious values are determined at the same time.
- Along each mesh line, two corresponding derivatives must be kept.
- Among the remaining four partial derivatives, eliminate two that are most difficult to evaluate according to the local geometry.

From Eq. (15), we have

$$\begin{pmatrix} u_\xi \\ u_\eta \\ u_\zeta \end{pmatrix} = \mathbf{P} \cdot \begin{pmatrix} u_x \\ u_y \\ u_z \end{pmatrix} \quad (20)$$

Therefore, Eqs. (19), (17) and (18) can be rewritten as

$$\begin{pmatrix} [\beta u_\xi] \\ [u_\eta] \\ [u_\zeta] \end{pmatrix} = \mathbf{C} \cdot \begin{pmatrix} u_x^+ \\ u_x^- \\ u_y^+ \\ u_y^- \\ u_z^+ \\ u_z^- \end{pmatrix} \quad (21)$$

where

$$\mathbf{C} = \begin{pmatrix} C_1 \\ C_2 \\ C_3 \end{pmatrix} = \begin{pmatrix} p_{11}\beta^+ & -p_{11}\beta^- & p_{12}\beta^+ & -p_{12}\beta^- & p_{13}\beta^+ & -p_{13}\beta^- \\ p_{21} & -p_{21} & p_{22} & -p_{22} & p_{23} & -p_{23} \\ p_{31} & -p_{31} & p_{32} & -p_{32} & p_{33} & -p_{33} \end{pmatrix}. \quad (22)$$

Here p_{ij} is the ij th entry of the transformation matrix \mathbf{C} and C_i denotes i th row of \mathbf{C} . After eliminating the l th and the m th elements of entry of the array $(u_x^+, u_x^-, u_y^+, u_y^-, u_z^+, u_z^-)^T$, Eq. (21) becomes

$$a[\beta u_\xi] + b[u_\eta] + c[u_\zeta] = (aC_1 + bC_2 + cC_3) \cdot \begin{pmatrix} u_x^+ \\ u_x^- \\ u_y^+ \\ u_y^- \\ u_z^+ \\ u_z^- \end{pmatrix} \quad (23)$$

where

$$\begin{aligned} a &= C_{2l}C_{3m} - C_{3l}C_{2m} \\ b &= C_{3l}C_{1m} - C_{1l}C_{3m} \\ c &= C_{1l}C_{2m} - C_{2l}C_{1m}. \end{aligned} \quad (24)$$

In practice, the two remaining jump conditions Eqs. (3) and (23) are used to determine a pair of fictitious values at the intersection point of the interface and each of the mesh line at a time.

3.2 General MIB scheme

Consider a geometry illustrated in Figure 6. The domains are denoted by Ω^+ and Ω^- . The interface intersects the k th y -mesh line at point (x_o, y_o, z_o) on the yz plane. For discretizing central derivatives, two fictitious values, $f_{i,j,k}$ and $f_{i,j+1,k}$, are to be determined on irregular grid points.

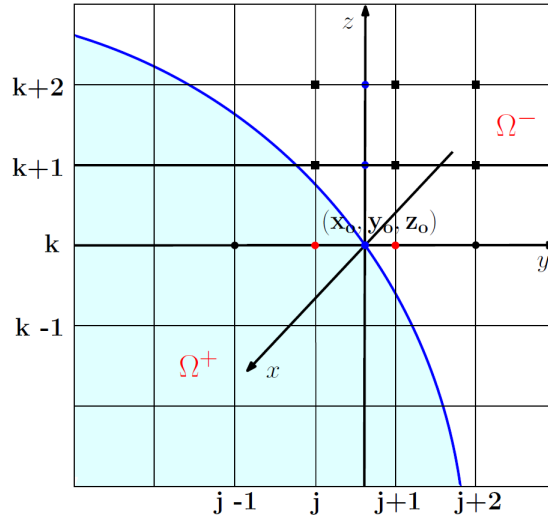


Figure 6: Smooth interface at cross section $x = x_i$. The interface intersects with the k th mesh line in the y direction at point (x_o, y_o, z_o) , where jump conditions need to be matched. At a pair of grid points in red color, namely (i, j, k) and $(i, j + 1, k)$, fictitious values are to be determined. Four grid points on the y mesh line are employed to approximate quantities at (x_o, y_o, z_o) , and six grid points denoted by black squares are employed to approximate $u_z^- |_{(x_o, y_o, z_o)}$.

Here, u^+ , u^- , u_y^+ and u_y^- at the intersection point (x_o, y_o, z_o) are easily expressed by interpolation

and the CFD scheme from information in Ω^+ and Ω^- , respectively

$$u^+ = (w_{0,j-1}, w_{0,j}, w_{0,j+1}) \cdot (u_{i,j-1,k}, u_{i,j,k}, f_{i,j+1,k})^T \quad (25)$$

$$u^- = (w_{0,j}, w_{0,j+1}, w_{0,j+2}) \cdot (f_{i,j,k}, u_{i,j+1,k}, u_{i,j+2,k})^T \quad (26)$$

$$u_y^+ = (w_{1,j-1}, w_{1,j}, w_{1,j+1}) \cdot (u_{i,j-1,k}, u_{i,j,k}, f_{i,j+1,k})^T \quad (27)$$

$$u_y^- = (w_{1,j}, w_{1,j+1}, w_{1,j+2}) \cdot (f_{i,j,k}, u_{i,j+1,k}, u_{i,j+2,k})^T, \quad (28)$$

where $w_{s,t}$ denote interpolation weights, which is generated by using the standard Lagrange polynomials [14]. The first subscript s represents either interpolation (when $s = 0$) or first order derivative (when $s = 1$) at point (x_o, y_o, z_o) , while the second subscript represents the node index.

We only need to compute two out of four remaining first order partial derivatives. For instance, if u_x^- and u_z^- are easily computed, then by choosing $s = 1$ and $t = 5$ in Eqs. (23) and (24), we can eliminate u_x^+ and u_z^+ .

To approximate u_z^+ or u_z^- , we need three more function values at the intersection points of the auxiliary line $y = y_o$ and the mesh line on the $y - z$ plane. Here we only provide a detailed scheme to approximate u_z^- , while other derivatives can be approximated in the same manner. Since these points are not on grid nodes, they are interpolated by nearby grid points along the y direction. Therefore, six more auxiliary points are involved. As illustrated in Figure 6, $u_z^-(x_o, y_o, z_o)$ can be approximately as

$$u_z^-(x_o, y_o, z_o) = (w_{1,k}, w_{1,k+1}, w_{1,k+2}) \cdot \begin{pmatrix} w_{0,j} & w_{0,j+1} & w_{0,j+2} & 0 & 0 & 0 & 0 & 0 & 0 \\ 0 & 0 & 0 & w'_{0,j} & w'_{0,j+1} & w'_{0,j+2} & 0 & 0 & 0 \\ 0 & 0 & 0 & 0 & 0 & 0 & w^*_{0,j} & w^*_{0,j+1} & w^*_{0,j+2} \end{pmatrix} \cdot \mathbf{U} \quad (29)$$

where $\mathbf{U} = (f_{i,j,k}, u_{i,j+1,k}, u_{i,j+2,k}, u_{i,j,k+1}, u_{i,j+1,k+1}, u_{i,j+2,k+1}, u_{i,j,k+2}, u_{i,j+1,k+2}, u_{i,j+2,k+2})^T$. Here the superscripts on w denotes different sets of FD weights [14]. Similarly, u_x^- can be approximated along the auxiliary line $y = y_o$ on the xy plane. Then jump conditions Eqs. (3) and (23) combined are used to solve the pair of fictitious values $f_{i,j,k}$ and $f_{i,j+1,k}$ at the same time. Consequently, the two fictitious values are expressed as a linear combination of 16 function values at nearby grid points and 4 jump conditions.

3.3 MIB scheme for interface with large curvatures

The above argument is based on a crucial assumption, which is that on each mesh line, there should be enough grid nodes (at least two for employing second order standard FD scheme) near the interface inside each subdomain so that the jump conditions can be expressed. However, when the curvature of the interface is very large, this assumption cannot be guaranteed for all mesh sizes.

As is illustrated in Figure 7, fictitious value $f_{i,j,k}$, $f_{i,j-1,k}$ and $f_{i,j+1,k}$ cannot be solved along y -direction, since there is only one grid point inside the interface in the y -direction. The concept of disassociation is introduced in Ref. [69] in order to disassociate the domain extension from the discretization thus broaden the applicability of the MIB method to general interface geometry. In the situation of Figure 7, we cannot solve the fictitious values in the y -direction, however, there is no problem to solve the fictitious values in the z -direction. Consequently, the fictitious value at an irregular point, regardless of the direction in its calculation, can be used for discretization in any direction involving the grid point without loss of accuracy. For fictitious values that can be obtained in multiple directions, we may compute their values in the most convenient manner and use them for necessary discretization. In practice, in order to make the MIB matrix as symmetric and banded as possible, if the fictitious value can be found in the given direction, one should use the fictitious value obtained from the corresponding direction and avoid using the disassociation technique. It is also worth of mentioning that disassociation technique does not reduce the accuracy of the numerical scheme. For instance, if fictitious values obtained from the z -direction has $O(h^m)$ accuracy for some integer m . This accuracy of approximation is independent of the direction in which the fictitious values are obtained. Here h is the grid size of the uniform mesh.

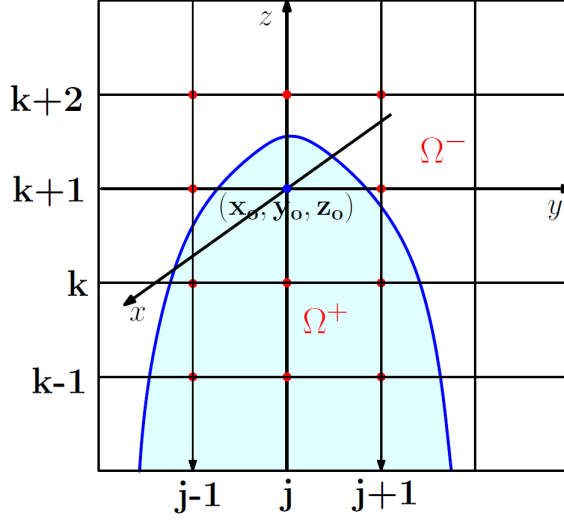


Figure 7: Disassociation type of irregular grid points at cross section $x = x_i$. Fictitious value need to be deployed at point (i, j, k) , $(i, j - 1, k)$ and $(i, j + 1, k)$ in order to discretize the PDE at these points. However, $f_{i,j,k}$, $f_{i,j-1,k}$ and $f_{i,j+1,k}$ can not be obtained from the y -direction by the general MIB scheme, since there are not enough points in Ω^+ . Luckily, these fictitious value can be obtained from the z -direction. For the above figure, during the discretization process, fictitious values obtained in the z -direction will be utilized for both the y -direction and the z -direction discretizations of the PDE.

Table 1: Numerical errors and convergence orders for a 6-petal flower interface problem (Case 1).

| $n_x \times n_y$ | $L_\infty(u)$ | Order | $L_2(u)$ | Order |
|------------------|---------------|-------|----------|-------|
| 40×40 | 3.790e-5 | | 1.910e-5 | |
| 80×80 | 4.867e-6 | 2.96 | 1.827e-6 | 3.38 |
| 160×160 | 8.545e-7 | 2.51 | 2.275e-7 | 2.99 |

4 Numerical studies

In this section, we examine validity and test the performance of the proposed MIB-FVM for solving the 3D Poisson equation with discontinuous coefficients. To demonstrate the robustness and accuracy of the present MIB-FVM, we carry out many numerical experiments with complex interfaces in both 2D and 3D settings. For 2D test cases, we start with a 6-petal flower shape interface which is relatively complex. The 2D jigsaw puzzle-like interface is also studied. For 3D problems, we consider various interface geometries including sphere, ellipsoid, cylinder, 5-petal flower and torus. Finally, we investigate our MIB-FVM's ability to deal with low regularity solutions in two more test cases.

Case 1. We first consider a 2D interface problem. The 2D Poisson equation is solved in domain $[-1, 1] \times [-1, 1]$. The interface of the problem is a 6-petal flower whose formula in polar coordinate system is given as $r = \frac{1}{2}(1 + \frac{1}{2} \sin(6\theta))$. The designed solution in two different domains are given by

$$u^+(x, y) = \frac{1}{4} + \sin(x) \sin(y), \quad \text{and} \quad u^-(x, y) = 0. \quad (30)$$

The coefficients are given by $\beta^+(x, y) = \beta^-(x, y) = 1$.

Figure 8 depicted the numerical solution and the L_∞ error on a $40 \times 40 \times 40$ mesh. From the plot of

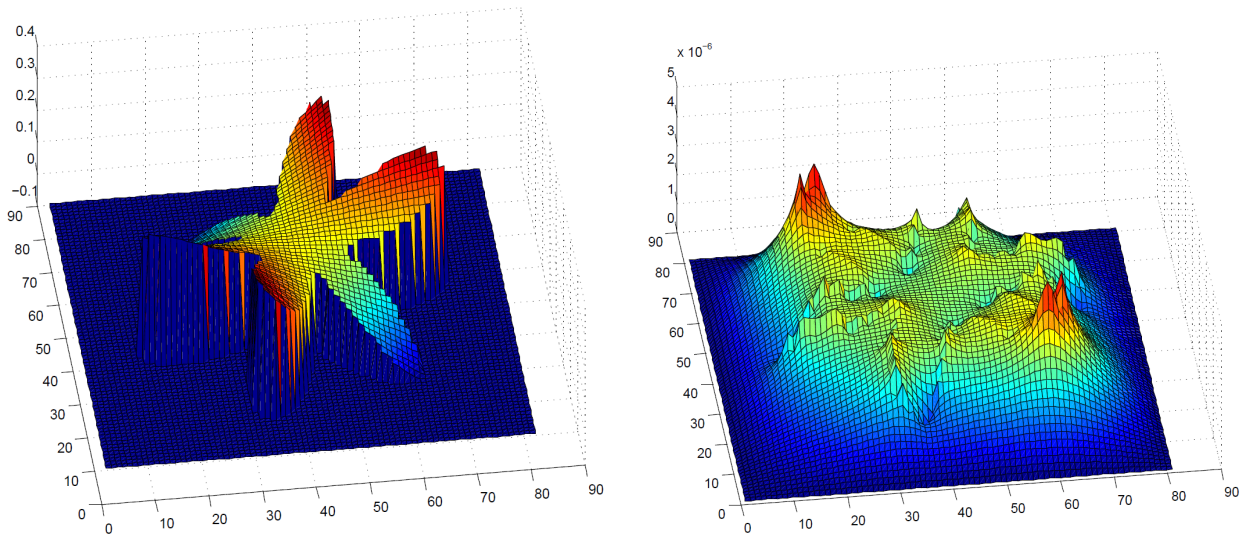


Figure 8: The computed solution on an 80×80 mesh (Left chart) and the L_∞ error (Right chart) for Case 1.

Table 2: Numerical errors and convergence orders for an ellipsoidal interface problem (Case 2).

| $n_x \times n_y$ | $L_\infty(u)$ | Order | $L_2(u)$ | Order |
|------------------|---------------|-------|----------|-------|
| 40×60 | 1.490e-3 | | 2.176e-4 | |
| 80×120 | 2.255e-4 | 2.72 | 3.654e-5 | 2.57 |
| 160×240 | 2.448e-5 | 3.20 | 4.067e-6 | 3.16 |

the L_∞ error on the right, it is noticed that the highest error appears at the tips of the petals, where the curvature of the interface is relatively higher. Table 1 shows the results of the numerical accuracy tests on three successively refined meshes. From the table, it can be seen that MIB-FVM obtains the second order accuracy in both the L_∞ error and L_2 error.

Case 2. We next consider the 2D jigsaw puzzle-like interface problem. The 2D Poisson equation is solved in domain $[-1, 1] \times [0, 3]$. The interface of the problem is a jigsaw puzzle-like shape whose formula is given as

$$\begin{cases} x(\theta) = 0.6 \cos(\theta) - 0.3 \cos(3\theta) \\ y(\theta) = 1.5 + 0.7 \sin(\theta) - 0.07 \sin(3\theta) + 0.2 \sin(7\theta) \end{cases} \quad (31)$$

The solution in two different subdomains is chosen as

$$u^+(x, y) = e^x(y^2 + x^2 \sin(y)), \quad \text{and} \quad u^-(x, y) = -(x^2 + y^2) \quad (32)$$

The discontinuous coefficients are given by $\beta^+(x, y, z) = 1$, and $\beta^-(x, y, z) = 10$.

Figure 9 depicted the computed solution and the L_∞ error on a $40 \times 40 \times 40$ mesh. The numerical errors in terms of L_∞ norm are collected in Table 2, which also show the second order convergence of the proposed MIB-FVM.

Case 3. Next we investigate a classical spherical interface problem. The 3D Poisson equation is solved in domain $[-1, 1] \times [-1, 1] \times [-1, 1]$. To specify the spherical interface, we design the level set

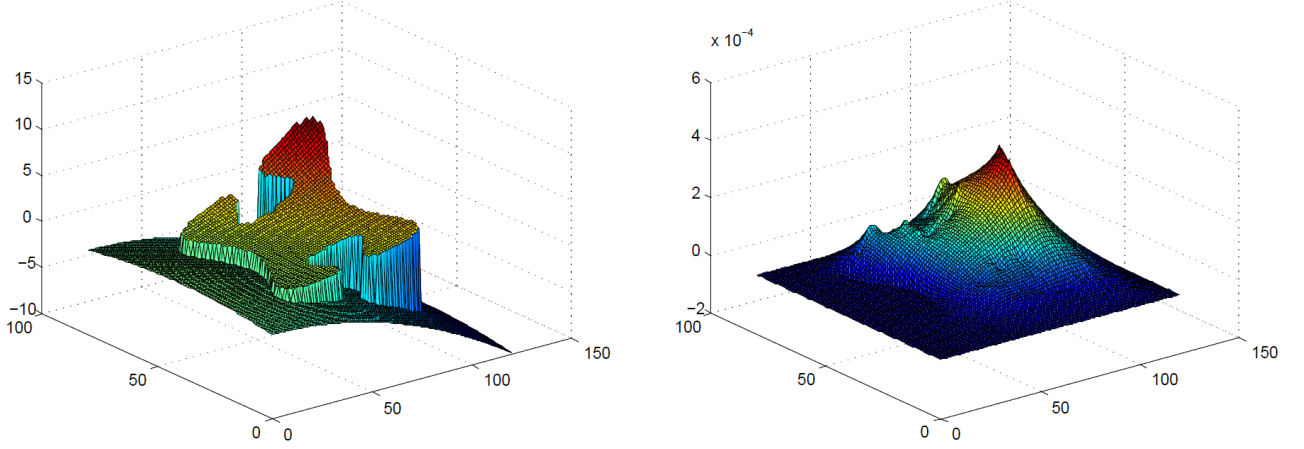


Figure 9: The computed solution on a 40×40 mesh (Left chart) and the L_∞ error (Right chart) for Case 2.

Table 3: Numerical errors and convergence orders for a spherical interface problem (Case 3(a)).

| $n_x \times n_y \times n_z$ | $L_\infty(u)$ | Order | $L_2(u)$ | Order |
|-----------------------------|---------------|-------|-----------|-------|
| $20 \times 20 \times 20$ | 1.2771e-3 | | 5.5733e-4 | |
| $40 \times 40 \times 40$ | 2.8944e-4 | 2.14 | 1.2612e-4 | 2.14 |
| $80 \times 80 \times 80$ | 6.4798e-6 | 2.15 | 2.8204e-5 | 2.16 |
| $160 \times 160 \times 160$ | 1.1673e-5 | 2.47 | 4.6283e-6 | 2.61 |

function $\phi(x, y, z)$

$$\phi(x, y, z) = r_0^2 - (x^2 + y^2 + z^2), \quad (33)$$

where the radius $r_0 = 3/4$. The interface is given as $\Gamma = \{(x, y, z) | \phi = 0, \forall (x, y, z) \in \Omega\}$. Two subdomains are $\Omega^+ = \{(x, y, z) | \phi \geq 0, \forall (x, y, z) \in \Omega\}$, and $\Omega^- = \{(x, y, z) | \phi < 0; \forall (x, y, z) \in \Omega\}$. The solution in two different subdomains is chosen as

$$u^+(x, y, z) = 0, \quad \text{and} \quad u^-(x, y, z) = \cos(x) \cos(y) \cos(z). \quad (34)$$

The discontinuous coefficients are given by

- **Case 3(a):**

$$\beta^+(x, y, z) = 8, \quad \text{and} \quad \beta^-(x, y, z) = 1. \quad (35)$$

- **Case 3(b):**

$$\beta^+(x, y, z) = 1 + \cos\left(\frac{x}{10} + \frac{y}{10} + \frac{z}{10}\right), \quad \text{and} \quad \beta^-(x, y, z) = 1 + 3 \sin\left(\frac{x}{10} + \frac{y}{10} + \frac{z}{10}\right). \quad (36)$$

Table 3 lists numerical results for the spherical interface problem. The geometry and error are depicted in Figure 10. It is seen that errors are very small at the fine mesh. The second order convergence is found.

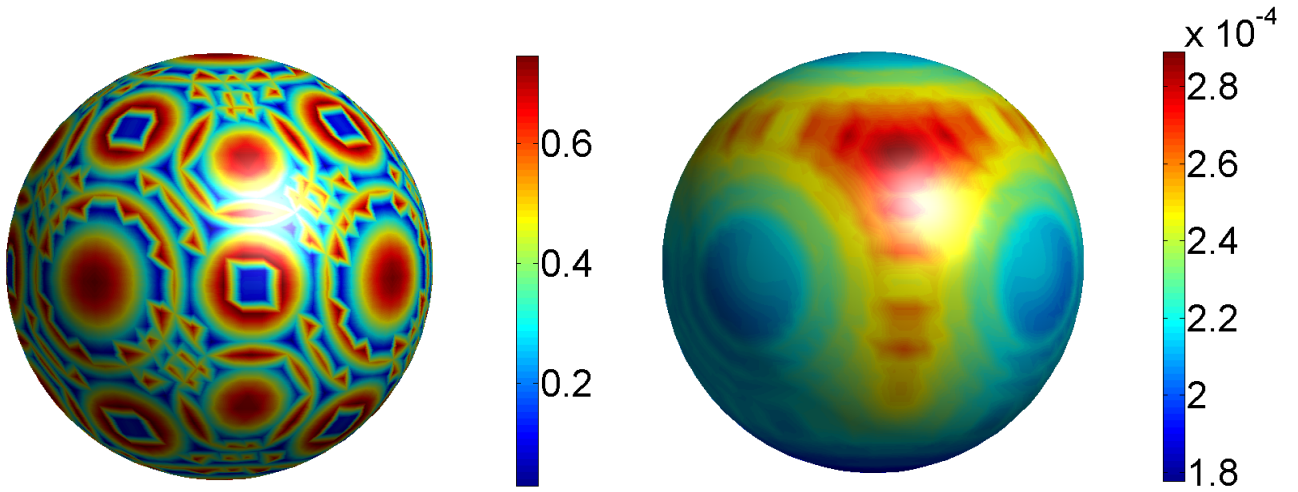


Figure 10: The computed solution on a $40 \times 40 \times 40$ mesh (Left chart) and the L_∞ error (Right chart) for Case 3(a).

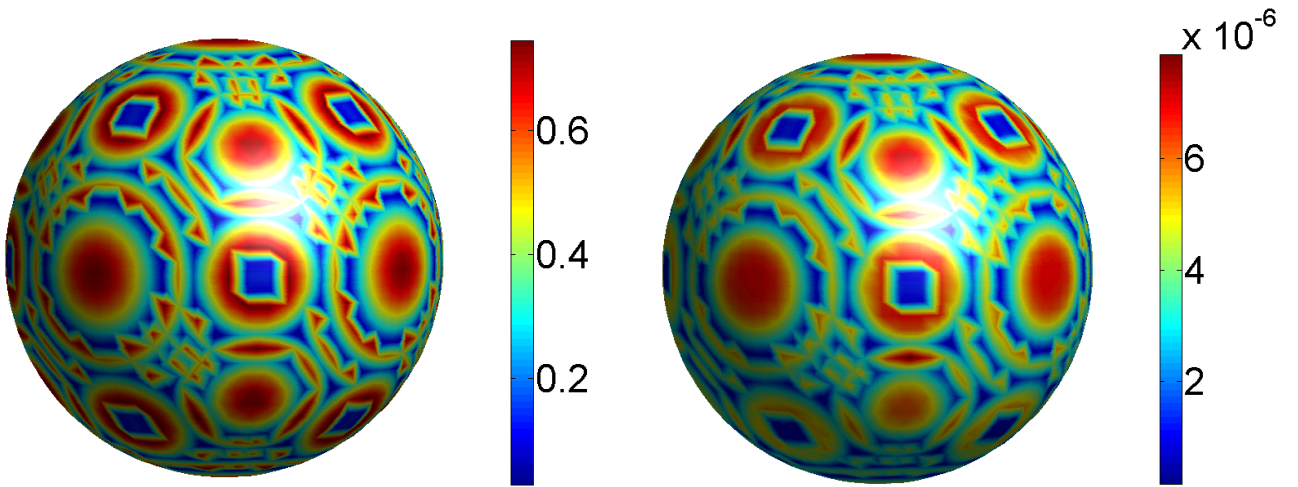


Figure 11: The computed solution on a $40 \times 40 \times 40$ mesh (Left chart) and the L_∞ error (Right chart) for Case 3(b).

Table 4: Numerical errors and convergence orders for a spherical interface problem (Case 3(b)).

| $n_x \times n_y \times n_z$ | $L_\infty(u)$ | Order | $L_2(u)$ | Order |
|-----------------------------|---------------|-------|-----------|-------|
| $20 \times 20 \times 20$ | 8.3466e-5 | | 3.0069e-5 | |
| $40 \times 40 \times 40$ | 1.9207e-5 | 2.12 | 6.8250e-6 | 2.14 |
| $80 \times 80 \times 80$ | 4.9351e-6 | 1.96 | 1.5630e-6 | 2.13 |
| $160 \times 160 \times 160$ | 1.5551e-6 | 1.67 | 3.7873e-7 | 2.05 |

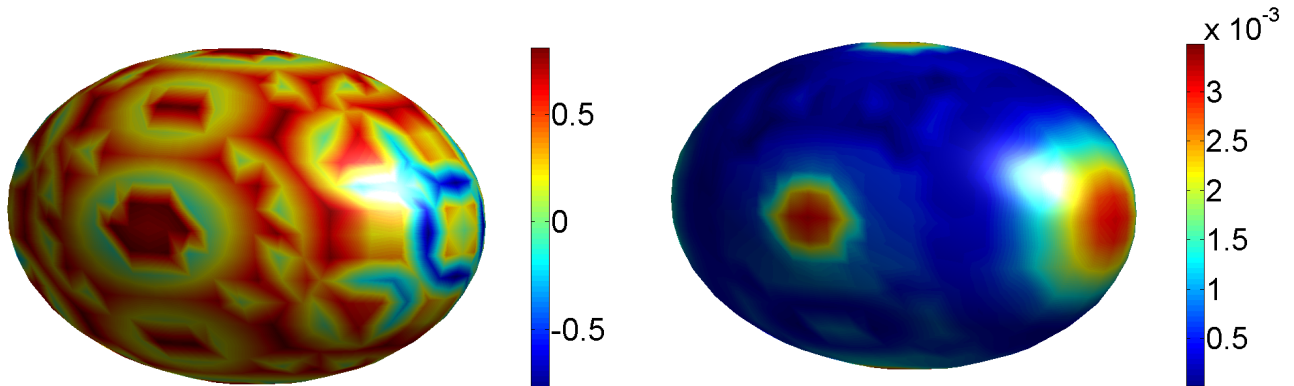


Figure 12: The computed solution on a $40 \times 40 \times 40$ mesh (Left chart) and the L_∞ error (Right chart) for Case 4.

Table 5: Numerical errors and convergence orders for an ellipsoidal interface problem (Case 4).

| $n_x \times n_y \times n_z$ | $L_\infty(u)$ | Order | $L_2(u)$ | Order |
|-----------------------------|---------------|-------|-----------|-------|
| $20 \times 20 \times 20$ | 2.1881e-2 | | 6.8115e-3 | |
| $40 \times 40 \times 40$ | 5.5719e-3 | 1.97 | 1.7463e-3 | 1.96 |
| $80 \times 80 \times 80$ | 1.4675e-3 | 1.92 | 4.5309e-4 | 1.95 |
| $160 \times 160 \times 160$ | 3.6068e-4 | 2.02 | 1.0974e-4 | 2.05 |

To further investigate the present method, we change the coefficient into a position dependent function in Case 3(b). Result is given in Table 4, which also demonstrates the second order accuracy in both L_∞ and L_2 norms for the solution.

Case 4. We next consider an ellipsoidal interface problem. The 3D Poisson equation is solved in domain $[-5, 5] \times [-5, 5] \times [-5, 5]$. The interface of the problem is an ellipsoid given as $\left(\frac{x}{7}\right)^2 + \left(\frac{y}{14}\right)^2 + \left(\frac{z}{25}\right)^2 = 1$. To specify the ellipsoidal interface, we define the level set function $\phi(x, y, z)$

$$\phi(x, y, z) = 1 - \left(\left(\frac{x}{7}\right)^2 + \left(\frac{y}{14}\right)^2 + \left(\frac{z}{25}\right)^2 \right) \quad (37)$$

The interface is given as $\Gamma = \{(x, y, z) | \phi = 0, \forall (x, y, z) \in \Omega\}$. Two subdomains are $\Omega^+ = \{(x, y, z) | \phi \geq 0, \forall (x, y, z) \in \Omega\}$, and $\Omega^- = \{(x, y, z) | \phi < 0; \forall (x, y, z) \in \Omega\}$. The solution in two different subdomains is chosen as

$$u^+(x, y, z) = e^{-\frac{x^2+y^2+z^2}{20}}, \quad \text{and} \quad u^-(x, y, z) = \cos(x) \cos(y) \cos(z). \quad (38)$$

The discontinuous coefficients are given by $\beta^+(x, y, z) = z + 15$, and $\beta^-(x, y, z) = \frac{x+y}{2} + 10$.

Figure 12 depicted the numerical solution and the L_∞ error on a $40 \times 40 \times 40$ mesh. From the result demonstrated in Table 5, it can be seen that the MIB-FVM obtains the second order accuracy.

Case 5. In Case 5, the 3D Poisson equation is solved in domain $[-4, 4] \times [-4, 4] \times [-2, 8.4]$. The interface of the problem is a cylinder of height 2π and base radius π . The designed solution in two different subdomains is chosen as

$$u^+(x, y, z) = x + y + z, \quad \text{and} \quad u^-(x, y, z) = \cos(x) \cos(y) \cos(z). \quad (39)$$

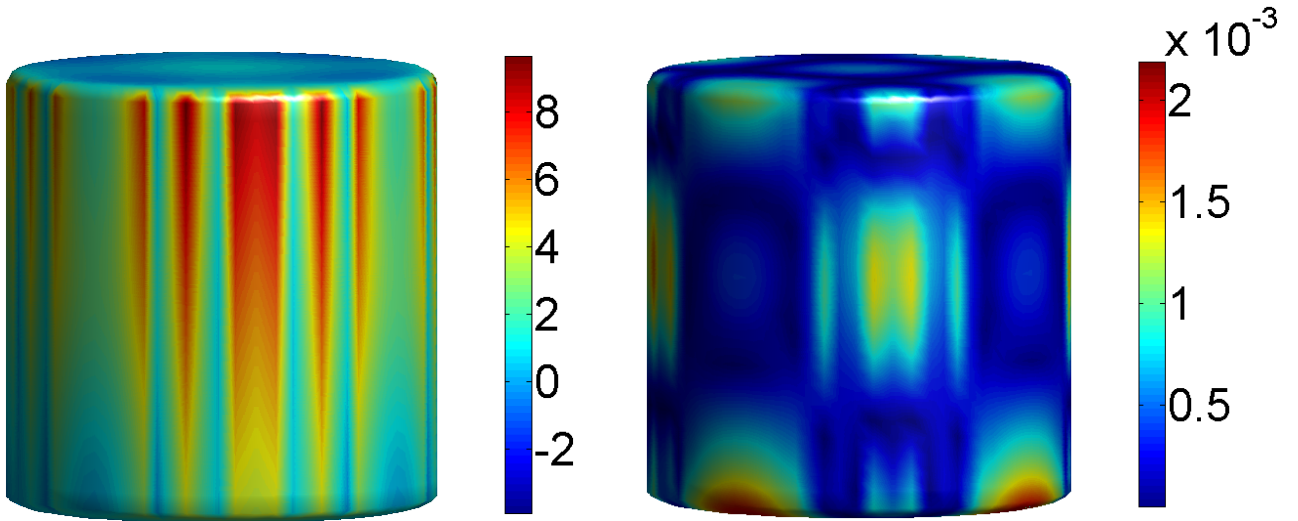


Figure 13: The computed solution on a $40 \times 40 \times 40$ mesh (Left chart) and the L_∞ error (Right chart) for Case 5.

Table 6: Numerical errors and convergence orders for a cylinder interface problem (Case 5).

| $n_x \times n_y \times n_z$ | $L_\infty(u)$ | Order | $L_2(u)$ | Order |
|-----------------------------|---------------|-------|-----------|-------|
| $20 \times 20 \times 20$ | 1.2274e-2 | | 2.9195e-3 | |
| $40 \times 40 \times 40$ | 3.0505e-3 | 2.01 | 7.7935e-4 | 1.91 |
| $80 \times 80 \times 80$ | 7.9267e-4 | 1.94 | 2.0674e-4 | 1.91 |
| $160 \times 160 \times 160$ | 1.8598e-4 | 2.09 | 4.6819e-5 | 2.14 |

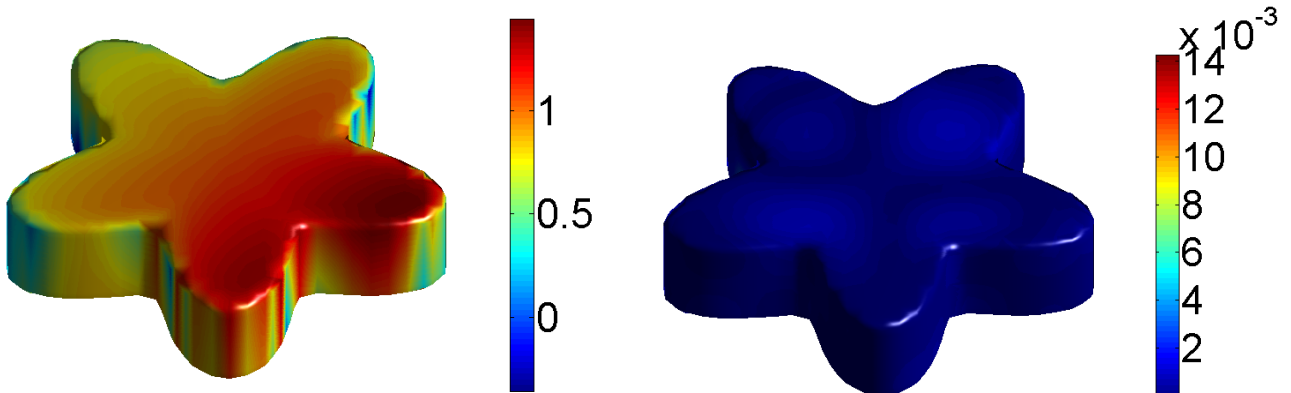


Figure 14: The computed solution on a $40 \times 40 \times 40$ mesh (Left chart) and the L_∞ error (Right chart) for Case 6.

Table 7: Numerical errors and convergence orders for a 5-petal flower-base cylinder interface problem (Case 6).

| $n_x \times n_y \times n_z$ | $L_\infty(u)$ | Order | $L_2(u)$ | Order |
|-----------------------------|---------------|-------|-----------|-------|
| $20 \times 20 \times 20$ | 4.9246e-2 | | 1.4819e-3 | |
| $40 \times 40 \times 40$ | 1.4307e-2 | 1.78 | 3.1350e-4 | 2.24 |
| $80 \times 80 \times 80$ | 4.9600e-4 | 4.85 | 5.6857e-5 | 2.46 |
| $160 \times 160 \times 160$ | 1.2096e-4 | 2.04 | 1.5637e-5 | 1.86 |

The discontinuous coefficients are given by $\beta^+(x, y, z) = 8$, and $\beta^-(x, y, z) = 1$.

Figure 13 depicted the numerical solution and the L_∞ error on a $40 \times 40 \times 40$ mesh. From the result demonstrated in Table 6, it can be seen that the proposed MIB-FVM achieves the second order accuracy.

Case 6. In Case 6, the 3D Poisson equation is solved in domain $[-5, 5] \times [-5, 5] \times [-2, 2]$. The interface of the problem is a 5-petal flower-base cylinder whose polar equation is given by $r = \frac{5}{2} + \frac{5}{7} \sin(5\theta)$ and $-\frac{2}{3} \leq z \leq \frac{2}{3}$. The designed solution in two different subdomains is chosen as

$$u^+(x, y, z) = \sin(x) \sin(y) \sin(z), \quad \text{and} \quad u^-(x, y, z) = e^{\frac{x}{10} + \frac{y}{10} + \frac{z}{10}}. \quad (40)$$

The discontinuous coefficients are given by $\beta^+(x, y, z) = 8$, and $\beta^-(x, y, z) = 1$.

Figure 14 depicted the numerical solution and the L_∞ error on a $40 \times 40 \times 40$ mesh. From the result demonstrated in Table 7, it can be seen that the present MIB-FVM obtains the second order accuracy.

Case 7. In Case 7, the 3D Poisson equation is solved in domain $[-5, 5] \times [-5, 5] \times [-2, 2]$. The interface of the problem is a torus whose equation is given by $(3 - \sqrt{x^2 + y^2})^2 + z^2 = 1$. The designed solution in two different subdomains is chosen as

$$u^+(x, y, z) = \sin(x) \sin(y) \sin(z) + 1, \quad \text{and} \quad u^-(x, y, z) = \cos(x) \cos(y) \cos(z). \quad (41)$$

The discontinuous coefficients are given by $\beta^+(x, y, z) = 8$, and $\beta^-(x, y, z) = 1$.

Figure 15 depicted the numerical solution and the L_∞ error on a $40 \times 40 \times 40$ mesh. From the result demonstrated in Table 8, it can be seen that the present MIB-FVM attains the second order accuracy.

Case 8. in this case, we test the proposed method for problems with low solution regularity.

- **Case 8(a):** The 3D Poisson equation is solved in domain $[-1, 1.05] \times [-1, 1.05] \times [-1, 1.05]$. The interface of the problem is a sphere the same as that in Case 3. The designed solution in two

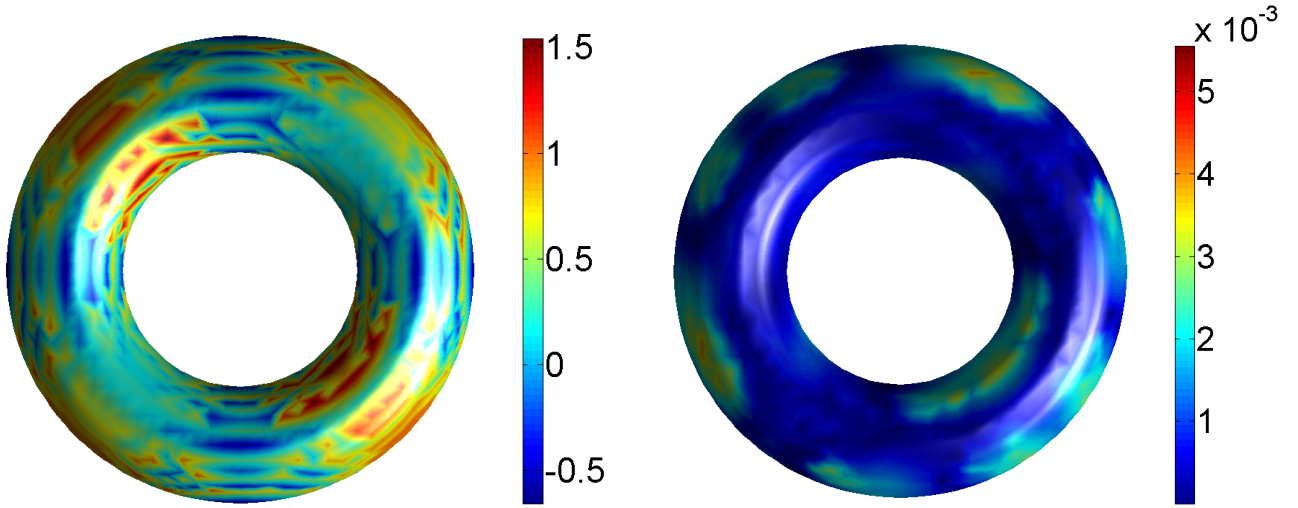


Figure 15: The computed solution on a $40 \times 40 \times 40$ mesh (Left chart) and the L_∞ error (Right chart) for Case 7.

Table 8: Numerical errors and convergence orders for a torus interface problem (Case 7).

| $n_x \times n_y \times n_z$ | $L_\infty(u)$ | Order | $L_2(u)$ | Order |
|-----------------------------|---------------|-------|-----------|-------|
| $20 \times 20 \times 20$ | 3.4040e-2 | | 4.6519e-3 | |
| $40 \times 40 \times 40$ | 5.7226e-3 | 2.57 | 1.0688e-3 | 2.12 |
| $80 \times 80 \times 80$ | 1.6415e-3 | 1.80 | 2.6468e-4 | 2.01 |
| $160 \times 160 \times 160$ | 3.8950e-4 | 2.08 | 6.9023e-5 | 1.94 |

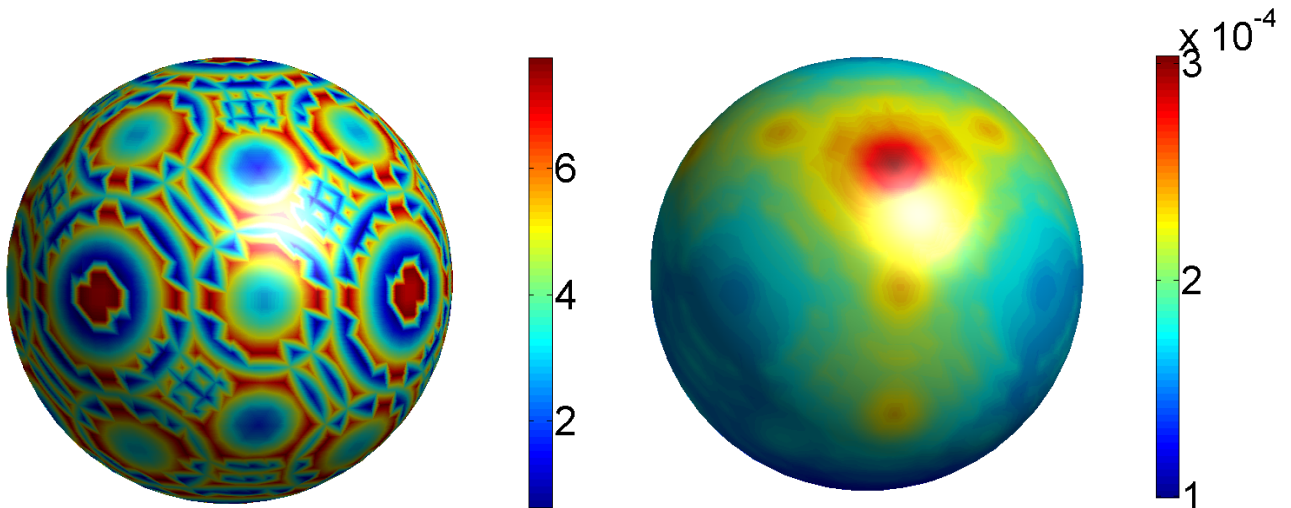


Figure 16: The computed solution on a $40 \times 40 \times 40$ mesh (Left chart) and the L_∞ error (Right chart) for Case 8(a).

Table 9: Numerical errors and convergence orders for a sphere interface problem (Case 8(a)).

| $n_x \times n_y \times n_z$ | $L_\infty(u)$ | Order | $L_2(u)$ | Order |
|-----------------------------|---------------|-------|-----------|-------|
| $20 \times 20 \times 20$ | 1.1578e-3 | | 3.3263e-4 | |
| $40 \times 40 \times 40$ | 3.0664e-4 | 1.92 | 9.2064e-5 | 1.85 |
| $80 \times 80 \times 80$ | 6.8400e-5 | 2.17 | 2.0947e-5 | 2.14 |
| $160 \times 160 \times 160$ | 1.3566e-5 | 2.34 | 4.4747e-6 | 2.24 |

different subdomains is chosen as

$$u^+(x, y, z) = 8, \quad \text{and} \quad u^-(x, y, z) = (x^2 + y^2 + z^2)^{\frac{5}{6}}. \quad (42)$$

The discontinuous coefficients are given by $\beta^+(x, y, z) = 4$, and $\beta^-(x, y, z) = 1$.

- **Case 8(b):** The 3D Poisson equation is solved in domain $[-5, 5.05] \times [-5, 5.05] \times [-5, 5.05]$. The interface of the problem is an ellipsoid the same as that in Case 4. The designed solution in two different subdomains is chosen as

$$u^+(x, y, z) = 8, \quad \text{and} \quad u^-(x, y, z) = (x^2 + y^2 + z^2)^{\frac{5}{6}} + \sin(x + y + z). \quad (43)$$

The discontinuous coefficients are given by $\beta^+(x, y, z) = z + 5$, and $\beta^-(x, y, z) = \frac{x+y}{2} + 10$.

In both cases, the second order derivatives of u_- blow up at the origin, making the solution only H^2 continuous in Ω^- . Since the differential form, Eq. (1), is of second order for the diffusion term, mathematically, Eq. (1) is invalid even though the underlying conservation law is still valid. However, it is noticed that the equivalent term in the integral form, Eq. (9), involves only the first order derivative. This reduction of the derivative order is important in dealing with solution which changes so rapidly in space that the spatial derivative does not exist. For these reasons, the finite volume method is preferred over the finite difference method in solving problems whose solution has less regularity and exhibits local discontinuities.

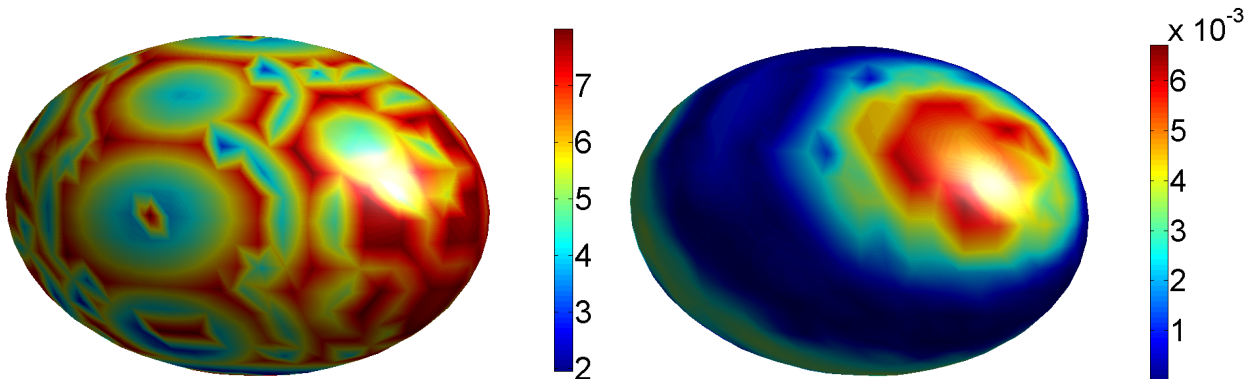


Figure 17: The computed solution on a $40 \times 40 \times 40$ mesh (Left chart) and the L_∞ error (Right chart) for Case 8(b).

Table 10: Numerical errors and convergence orders for an ellipsoid interface problem (Case 8(b)).

| $n_x \times n_y \times n_z$ | $L_\infty(u)$ | Order | $L_2(u)$ | Order |
|-----------------------------|---------------|-------|-----------|-------|
| $20 \times 20 \times 20$ | 3.2934e-2 | | 1.1797e-2 | |
| $40 \times 40 \times 40$ | 7.5420e-3 | 2.13 | 2.9620e-3 | 1.99 |
| $80 \times 80 \times 80$ | 1.9183e-3 | 1.98 | 7.5382e-4 | 1.97 |
| $160 \times 160 \times 160$ | 4.7448e-4 | 2.02 | 1.8701e-4 | 2.01 |

In Case 8(a), we choose constant diffusive coefficients β^+ and β^- , whereas in Case 8(b), β^+ and β^- are both position dependent. The numerical solutions and the L_∞ errors of Case 8(a) and Case 8(b) are depicted in Figure 16 and Figure 17, respectively. From the numerical results collected in Table 9 and Table 10, it is seen that the second order accuracy in both cases are essentially obtained.

5 Conclusion

In this work, we introduce the finite volume formulation of matched interface and boundary method (MIB-FVM) for solving elliptic interface problems arising from modeling material interface in practice. Much effort has been taken to develop advanced numerical schemes for such problems in the past few decades. However, challenges still remain in this field. One of the challenge concerns the development of methods with higher order accuracy. Another challenge is to develop methods for dealing with complex interface geometries. The matched interface and boundary (MIB) method has been proved to be able to deal with these challenges. However, since the MIB method is based on the collocation formulation, it does not work well for solutions with low regularity. Based on the integral form rather than the differential form, the finite volume method (FVM) is known for being able to deal with problems with low regularity solutions and better conserve mass and flux. Second order finite volume methods have also been formulated in literature for elliptic interface problems. Motivated by these successes, we propose the present MIB-FVM to take the advantages of MIB and FVM.

To reduce the computational cost of mesh generation, we utilize the Cartesian mesh, although the proposed MIB-FVM can be realized on irregular meshes as well. We also employ the vertex-centered FVM, for which the cubic control volumes are associated with the grid point at the center. The control volumes are categorized into regular and irregular types, where special treatments of the MIB formulation are needed for the irregular ones in order to maintain the designed accuracy. We study the proposed MIB-

FVM by a number of classical test cases, including both 2D cases such as 6-petal flower and jigsaw-puzzle like shape, and 3D cases such as sphere, ellipsoid, standard cylinder, flower-based cylinder and torus. The numerical results all demonstrate the second order accuracy of the proposed method. The ability of handling interface with complex geometries and solutions with low regularity (H^2 continuous) indicates that the proposed MIB-FVM combines the advantage of both MIB and FVM in meeting numerical challenges. Future work will be done to improve the present method in dealing with even more complex interface geometries, for example, interface with geometric singularities which are commonly seen in practical applications such as electrostatic analysis of proteins.

Acknowledgments

This work was supported in part by NSF grants IIS-1302285 and DMS-1160352, NIH Grant R01GM-090208, and MSU Center for Mathematical Molecular Biosciences Initiative.

References

- [1] L. Adams and Z. L. Li. The immersed interface/multigrid methods for interface problems. *SIAM J. Sci. Comput.*, 24:463–479, 2002.
- [2] H. B. Ameer, M. Burger, and B. Hackl. Level set methods for geometric inverse problems in linear elasticity. *Inverse Problems*, 20(3):673–696, 2004.
- [3] P. Bastian and C. Engwer. An unfitted finite element method using discontinuous Galerkin. *Int. J. Numer. Meth. Engng.*, 79:1557–1576, 2009.
- [4] J. T. Beale and A. T. Layton. On the accuracy of finite difference methods for elliptic problems with interfaces. *Comm. Appl. Math. Comp. Sci.*, 1:91–119, 2006.
- [5] P. A. Berthelsen. A decomposed immersed interface method for variable coefficient elliptic equations with non-smooth and discontinuous solutions. *J. Comput. Phys.*, 197(1):364–386, 2004.
- [6] W. Cai and S. Z. Deng. An upwinding embedded boundary method for Maxwell’s equations in media with material interfaces: 2d case. *J. Comput. Phys.*, 190:159–183, 2003.
- [7] D. Chen, Z. Chen, C. Chen, W. H. Geng, and G. W. Wei. MIBPB: A software package for electrostatic analysis. *J. Comput. Chem.*, 32:657 – 670, 2011.
- [8] D. Chen and W. W. Guo. Modeling and simulation of electronic structure, material interface and random doping in nano-electronic devices. *J. Comput. Phys.*, 229:4431–4460, 2010.
- [9] D. Chen and G. W. Wei. Modeling and simulation of electronic structure, material interface and random doping in nano-electronic devices. *J. Comput. Phys.*, 229:4431–4460, 2010.
- [10] M. A. Dumett and J. P. Keener. An immersed interface method for solving anisotropic elliptic boundary value problems in three dimensions. *SIAM Journal on Scientific Computing*, 25(1):348–367, 2003.
- [11] E. A. Fadlun, R. Verzicco, P. Orlandi, and J. Mohd-Yusof. Combined immersed-boundary finite-difference methods for three-dimensional complex flow simulations. *J. Comput. Phys.*, 161(1):35–60, 2000.
- [12] R. P. Fedkiw, T. Aslam, B. Merriman, and S. Osher. A non-oscillatory Eulerian approach to interfaces in multimaterial flows (the ghost fluid method). *J. Comput. Phys.*, 152:457–492, 1999.
- [13] A. L. Fogelson and J. P. Keener. Immersed interface methods for neumann and related problems in two and three dimensions. *SIAM Journal on Scientific Computing*, 22(5):1630–1654, 2001.
- [14] B. Fornberg. Calculation of weights in finite difference formulas. *SIAM Rev*, 40:685–691, 1998.
- [15] M. Francois and W. Shyy. Computations of drop dynamics with the immersed boundary method, part 2: Drop impact and heat transfer. *Numer. Heat Trans. Part B-Fund.*, 44, 2003.
- [16] W. Geng, S. Yu, and G. W. Wei. Treatment of charge singularities in implicit solvent models. *Journal of Chemical Physics*, 127:114106, 2007.
- [17] B. E. Griffith and C. S. Peskin. On the order of accuracy of the immersed boundary method: Higher order convergence rates for sufficiently smooth problems. *J. Comput. Phys.*, 208:75–105, 2005.

- [18] G. Guyomarch, C. O. Lee, and K. Jeon. A discontinuous galerkin method for elliptic interface problems with application to electroporation. In *Commun. Numer. Meth. Engng*, volume 25, pages 991–1008, 2009.
- [19] G. R. Hadley. High-accuracy finite-difference equations for dielectric waveguide analysis i: uniform regions and dielectric interfaces. *Journal of Lightwave Technology*, 20:1210–1218, 2002.
- [20] J. L. Hellrung Jr., L. M. Wang, E. Sifakis, and J. M. Teran. A second order virtual node method for elliptic problems with interfaces and irregular domains in three dimensions. *Journal of Computational Physics*, 231:2015–2048, 2012.
- [21] J. S. Hesthaven. High-order accurate methods in time-domain computational electromagnetics. a review. *Advances in Imaging and Electron Physics*, 127:59–123, 2003.
- [22] T. P. Horikis and W. L. Kath. Modal analysis of circular bragg fibers with arbitrary index profiles. *Optics Lett.*, 31:3417–3419, 2006.
- [23] S. Hou and X.-D. Liu. A numerical method for solving variable coefficient elliptic equation with interfaces. *J. Comput. Phys.*, 202(2):411–445, 2005.
- [24] T. Y. Hou, Z. L. Li, S. Osher, and H. K. Zhao. A hybrid method for moving interface problems with application to the heleshaw flow. *J. Comput. Phys.*, 134(2):236–252, 1997.
- [25] G. Iaccarino and R. Verzicco. Immersed boundary technique for turbulent flow simulations. *Appl. Mech. Rev.*, 56:331–347, 2003.
- [26] S. Jin and X. Wang. Robust numerical simulation of porosity evolution in chemical vapor infiltration: II. two-dimensional anisotropic fronts. *J. Comput. Phys.*, 179(2):557–577, 2002.
- [27] H. Johansen and P. Colella. A Cartesian grid embedded boundary method for Poisson’s equation on irregular domains. *J. Comput. Phys.*, 147(1):60–85, 1998.
- [28] R. Kafafy, T. Lin, Y. Lin, and J. Wang. Three-dimensional immersed finite element methods for electric field simulation in composite materials. *Int. J. Numer. Methods Engng.*, 64:940–972, 2005.
- [29] J. D. Kandilarov. Immersed interface method for a reaction-diffusion equation with a moving own concentrated source. In *NMA ’02: Revised Papers from the 5th International Conference on Numerical Methods and Applications*, pages 506–513, London, UK, 2003. Springer-Verlag.
- [30] M. C. Lai and C. S. Peskin. An immersed boundary method with formal second-order accuracy and reduced numerical viscosity. *J. Comput. Phys.*, 160:705–719, 2000.
- [31] A. T. Layton. Using integral equations and the immersed interface method to solve immersed boundary problems with stiff forces. *Comput. Fluids.*, 38:266–272, 2009.
- [32] L. Lee and R. J. LeVeque. An immersed interface method for incompressible navier–stokes equations. *SIAM Journal on Scientific Computing*, 25(3):832–856, 2003.
- [33] R. J. LeVeque and Z. L. Li. The immersed interface method for elliptic equations with discontinuous coefficients and singular sources. *SIAM J. Numer. Anal.*, 31:1019–1044, 1994.
- [34] Z. L. Li and K. Ito. Maximum principle preserving schemes for interface problems with discontinuous coefficients. *SIAM J. Sci. Comput.*, 23:339–361, 2001.
- [35] Z. L. Li, T. Lin, and X. H. Wu. New Cartesian grid methods for interface problems using the finite element formulation. *Numerische Mathematik*, 96:61–98, 2003.
- [36] M. N. Linnick and H. F. Fasel. A high-order immersed interface method for simulating unsteady incompressible flows on irregular domains. *J. Comput. Phys.*, 204(1):157–192, 2005.
- [37] W. K. Liu, Y. Liu, D. Farrell, L. Zhang, X. Wang, Y. Fukui, N. Patankar, Y. Zhang, C. Bajaj, X. Chen, and H. Hsu. Immersed finite element method and its applications to biological systems. *Computer Methods in Applied Mechanics and Engineering*, 195:1722–1749, 2006.
- [38] X. D. Liu, R. P. Fedkiw, and M. Kang. A boundary condition capturing method for Poisson’s equation on irregular domains. *J. Comput. Phys.*, 160:151–178, 2000.
- [39] B. Lombard and J. Piraux. How to incorporate the spring-mass conditions in finite-difference schemes. *SIAM Journal on Scientific Computing*, 24(4):1379–1407, 2003.
- [40] A. Mayo. The fast solution of Poisson’s and the biharmonic equations on irregular regions. *SIAM J. Numer. Anal.*, 21:285–299, 1984.

- [41] A. McKenney, L. Greengard, and A. Mayo. A fast Poisson solver for complex geometries. *J. Comput. Phys.*, 118:348–355, 1995.
- [42] G. Morgenthal and J. H. Walther. An immersed interface method for the vortex-in-cell algorithm. *Computers & Structures*, 85(11-14):712–726, 2007.
- [43] L. Mu, J. Wang, G. W. Wei, X. Ye, and S. Zhao. Weak Galerkin method for second order elliptic interface problems. *Journal of Computational Physics*, 250:106 – 125, 2013.
- [44] M. Overmann and R. Klein. A Cartesian grid finite volume method for elliptic equations with variable coefficients and embedded interfaces. *J. Comput. Phys.*, 219:749769, 2006.
- [45] C. S. Peskin. Numerical analysis of blood flow in the heart. *J. Comput. Phys.*, 25(3):220–52, 1977.
- [46] M. Schulz and G. Steinebach. Two-dimensional modelling of the river Rhine. *Journal of Computational and Applied Mathematics*, 145(1):11–20, 2002.
- [47] J. A. Sethian. Evolution, implementation, and application of level set and fast marching methods for advancing fronts. *J. Comput. Phys.*, 169(2):503–555, 2001.
- [48] M. Sussaman, P. Smereka, and S. Osher. A level set approach for computing solutions to incompressible two-phase flow. *J. Comput. Phys.*, 114:146–154, 1994.
- [49] A.-K. Tornberg and B. Engquist. Numerical approximations of singular source terms in differential equations. *J. Comput. Phys.*, 200(2):462–488, 2004.
- [50] J. J. Vande Voorde, J. Vierendeels, and E. Dick. Flow simulations in rotary volumetric pumps and compressors with the fictitious domain method. *Journal of Computational and Applied Mathematics*, 168(1-2):491–499, 2004.
- [51] B. Wang, K. L. Xia, and G. W. Wei. Matched interface and boundary method for elastic interface problems. *Journal of Computational and Applied Mathematics*, 285:203–225, 2015.
- [52] B. Wang, K. L. Xia, and G. W. Wei. Second order method for solving 3d elasticity equations with complex interfaces. *Journal of Computational Physics*, 294:405–438, 2015.
- [53] G. W. Wei. Discrete singular convolution for the solution of the Fokker-Planck equations. *J. Chem. Phys.*, 110:8930–8942, 1999.
- [54] G. W. Wei, Y. B. Zhao, and Y. Xiang. Discrete singular convolution and its application to the analysis of plates with internal supports, I theory and algorithm. *Int. J. Numer. Methods Engng.*, 55:913 – 946, 2002.
- [55] A. Wiegmann and K. P. Bube. The explicit-jump immersed interface method: Finite difference methods for PDEs with piecewise smooth solutions. *SIAM Journal on Numerical Analysis*, 37(3):827–862, 2000.
- [56] K. L. Xia and G. W. Wei. A Galerkin formulation of the MIB method for three dimensional elliptic interface problems. *Computers and Mathematics with Applications*, 68:719–745, 2014.
- [57] K. L. Xia, M. Zhan, D. C. Wan, and G. W. Wei. Adaptively deformed mesh based matched interface and boundary (MIB) method for elliptic interface problems. *Journal of Computational Physics*, 231:1440–1461, 2012.
- [58] K. L. Xia, M. Zhan, and G.-W. Wei. The matched interface and boundary (MIB) method for multi-domain elliptic interface problems. *Journal of Computational Physics*, 230:8231–8258, 2011.
- [59] K. L. Xia, M. Zhan, and G. W. Wei. MIB Galerkin method for elliptic interface problems. *Journal of Computational and Applied Mathematics*, 272:195–220, 2014.
- [60] S. N. Yu, W. H. Geng, and G. W. Wei. Treatment of geometric singularities in implicit solvent models. *Journal of Chemical Physics*, 126:244108, 2007.
- [61] S. N. Yu and G. W. Wei. Three-dimensional matched interface and boundary (MIB) method for treating geometric singularities. *J. Comput. Phys.*, 227:602–632, 2007.
- [62] S. N. Yu, Y. Xiang, and G. W. Wei. Matched interface and boundary (mib) method for the vibration analysis of plates. *Commun. Numer. Methods Engng*, 25:923–950, 2009.
- [63] S. N. Yu, Y. C. Zhou, and G. W. Wei. Matched interface and boundary (MIB) method for elliptic problems with sharp-edged interfaces. *J. Comput. Phys.*, 224(2):729–756, 2007.
- [64] S. Zhao. Full-vectorial matched interface and boundary (MIB) method for the modal analysis of dielectric waveguides. *IEEE/OSA Journal of Lightwave Technology*, 26:2251–2259, 2008.

- [65] S. Zhao. High order matched interface and boundary methods for the Helmholtz equation in media with arbitrarily curved interfaces. *J. Comput. Phys.*, 229:3155–3170, 2010.
- [66] S. Zhao and G. W. Wei. High-order FDTD methods via derivative matching for Maxwell’s equations with material interfaces. *J. Comput. Phys.*, 200(1):60–103, 2004.
- [67] Y. C. Zhou, M. Feig, and G. W. Wei. Highly accurate biomolecular electrostatics in continuum dielectric environments. *Journal of Computational Chemistry*, 29:87–97, 2008.
- [68] Y. C. Zhou, J. G. Liu, and D. L. Harry. A matched interface and boundary method for solving multi-flow navier-stokes equations with applications to geodynamics. *Journal of Computational Physics*, 231:223–242, 2012.
- [69] Y. C. Zhou and G. W. Wei. On the fictitious-domain and interpolation formulations of the matched interface and boundary (MIB) method. *J. Comput. Phys.*, 219(1):228–246, 2006.
- [70] Y. C. Zhou, S. Zhao, M. Feig, and G. W. Wei. High order matched interface and boundary method for elliptic equations with discontinuous coefficients and singular sources. *J. Comput. Phys.*, 213(1):1–30, 2006.